PHOTONICS Research

Transmissive metasurface for multi-channel and full-polarization modulation of electromagnetic wavefronts

Linda Shao,[1,†] Zhenfei Li,[1,†] Jialin Feng,[2] Jin Zhang,[1] Hongyu Shi,[2] Xudong Bai,[3,4] and Weiren Zhu[1,*]

[1]Department of Electronic Engineering, Shanghai Jiao Tong University, Shanghai 200240, China
[2]School of Information and Communications Engineering, Xi'an Jiaotong University, Xi'an 710049, China
[3]School of Microelectronics, Northwestern Polytechnical University, Taicang 215400, China
[4]e-mail: baixudong@nwpu.edu.cn
*Corresponding author: weiren.zhu@sjtu.edu.cn

Received 12 September 2022; revised 14 December 2022; accepted 14 December 2022; posted 15 December 2022 (Doc. ID 475364); published 1 February 2023

Metasurfaces have great potential for flexible manipulation of electromagnetic wave polarizations and wavefronts. Here, we propose a general method for achieving independent wavefront manipulation in a single polarization-multiplexing transmissive metasurface. As a proof of concept, we design a transmission-type anisotropic metasurface for independent wavefront manipulation in full-polarization channels. An *x*-polarized wave transmitted through such a metasurface could be converted into four outgoing beams with delicately designed polarization states that converge to specific positions for holographic imaging. The measured results are in good agreements with simulated ones, verifying the independent wavefront manipulations with arbitrary polarization conversions. Compared with the existing traditional meta-devices with single-polarization modulation, we achieve polarization-multiplexed metasurfaces with mixed polarization and phase control, which can greatly improve the functional richness of the system.

https://doi.org/10.1364/PRJ.475364

1. INTRODUCTION

Metamaterials are composed of subwavelength artificial meta-atoms with periodic or aperiodic arrangements, possessing many exotic properties in flexibly manipulating electromagnetic waves [1,2]. Based on metamaterials, many exceptional phenomena and fantastic devices have been reported such as negative refraction [3,4], invisible cloaks [5,6], and perfect absorption [7]. Unlike three-dimensional metamaterials, metasurfaces are two-dimensional planar metamaterials and have the advantages of small size, easy fabrication, and low loss as well as powerful capabilities in multiple field dimensions of electromagnetic waves, such as phase control [8–11], amplitude modulation [12,13], polarization control [14,15], and frequency control [16,17].

The efficient and versatile control of electromagnetic wave polarization has been increasingly demanded in various applications in multi-functional wavefront manipulation [18], electromagnetic multiplexing [19], and encryption [20]. Due to disadvantages such as large volume, difficult design, and high processing requirements of traditional polarization converters, metasurface polarization converters with artificially strong anisotropy have been proposed in recent years [21–24]. In addition, with the rapid development of miniaturized and highly integrated information systems, it is increasingly necessary to promote the design of multi-functional equipment in many applications. In the reported research on polarization multiplexed multifunctional metasurfaces, a class of metasurfaces can have different functions according to the incident polarization states [18,25]. On the other hand, metasurfaces can also realize multiple independent functions in different polarization channels at the same time [26,27]. However, most of the previously reported metasurfaces can only work in a few polarized channels in the transmission space, such as left-handed circular polarization (LCP) and right-handed circular polarization (RCP) dual channels. They also do not have the ability to manipulate different polarizations and wavefronts independently in the transmission space simultaneously. At present, there have been reports about multi-channel electromagnetic wave manipulation based on reflection-type metasurfaces [27]. Although it is easy to achieve very high work efficiency with reflective metasurfaces, they are not suitable for some occasions with specific requirements. Therefore, this work is extended to the transmission-type metasurface.

In this work, we propose a general strategy to realize independent phase and polarization manipulation based on multi-beam transmissive metasurfaces. This strategy only needs us to adjust the two orthogonal propagation phases of each anisotropic meta-atom. The simulation results show that the transmitted electromagnetic wave has four independent information channels at the same time, and the transmitted energy converges to different positions of the holographic image. A prototype of the metasurface is fabricated, and the polarization multiplexing hologram is experimentally realized at 26 GHz. The experimental results are in good agreement with the simulation ones.

2. THEORETICAL ANALYSIS AND META-ATOM DESIGN

A typical transmission metasurface hologram system at the microwave frequency is schematically shown in Fig. 1. Multiple beams are generated when an x-polarized beam transmits through the metasurface, where each outgoing beam could be independently controlled in terms of both wavefront and polarization.

We consider an anisotropic meta-atom exhibiting mirror symmetry along both the x and y directions. Considering that a linearly polarized plane wave is normally incident along the z axis upon a transmission-type unit cell at the xoy plane with the electric polarization 45° off the x axis, the electric field vector of the incident plane wave E_i can be decomposed into x and y components, and the transmitted field E_t can be expressed as

$$E_t = \frac{|E_i|}{\sqrt{2}} t_{xx} e^{j\phi_{xx}} e^{jkz} \hat{x} + \frac{|E_i|}{\sqrt{2}} t_{yy} e^{j\phi_{yy}} e^{jkz} \hat{y}, \tag{1}$$

where t_{xx} and ϕ_{xx} denote the transmission amplitude and phase along the x direction, and t_{yy} and ϕ_{yy} denote the transmission amplitude and phase along the y direction. Assuming $t_{xx} = t_{yy} = t$, we thus have

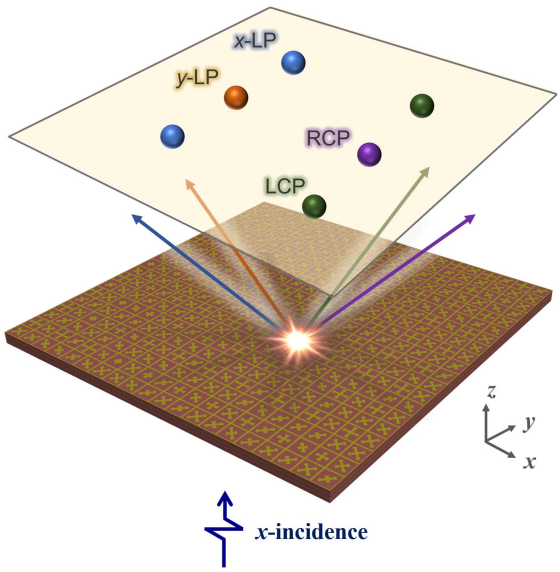

Fig. 1. Conceptual configuration of multi-focus meta-hologram with multi-channel transmission.

$$E_t = \frac{E_0}{\sqrt{2}} t e^{jkz} e^{j\phi_{xx}} \left[\hat{x} + e^{j(\phi_{yy}-\phi_{xx})}\hat{y}\right], \tag{2}$$

where $\Delta\phi = \phi_{yy} - \phi_{xx}$ is the phase difference. The polarization states can be flexibly manipulated for different phase differences $\Delta\phi$ controlled by the designed unit cells. For the case in which the phase difference meets $\Delta\phi = 2n\pi$, when n is an even number, a transmission with the same polarization will be obtained; when n is odd, an orthogonal polarization transmission will be obtained. Meanwhile, when $\Delta\phi = 2n\pi \pm \pi/2$, the transmitted wave will become a circularly polarized wave, where "+" indicates LCP and "−" indicates RCP. As we can see from Eq. (2), in addition to manipulating the polarization of the transmitted wave, its phase response can be manipulated independently by controlling ϕ_{xx}. Therefore, under a 45° linearly polarized incidence, the transmission characteristics of the metasurface are jointly determined by the transmission phase response (ϕ_{xx}) and polarization state of the wave ($\Delta\phi$). In other words, the wavefront and polarization of the transmitted electromagnetic waves can be controlled independently by a predesigned metasurface.

As a consequence, the key point of our work is constructing the propagation kernel and properly designing the unit cells based on the just discussed theoretical analysis. The unit cell requires a free control of the two phase responses ϕ_{xx} and ϕ_{yy} for linear incidence. In this work, based on the principle of cascading multilayer structures [28], we select a four-layer structure metasurface unit to meet the demand and realize polarization multiplexing. The metasurface unit covers the required phase range and keeps the transmission amplitude at a relatively high level. The 3D view and top view of the designed unit cell are illustrated in Figs. 2(a) and 2(b). The unit cell consists of four layers of copper (0.018 mm thickness) with the same structure and three layers of F4B ($\varepsilon = 2.65$, $\tan\delta = 0.001$, 1.5 mm thickness). The periodicity of the unit cell is $p = 3$ mm. The orthogonal I-shaped resonant structure on the metal layer is placed along the x and y axes. Two transmission phase responses ϕ_{xx} and ϕ_{yy} vary with the length l_x and l_y. The peripheral metal frame isolates the unit to reduce the coupling of adjacent unit cells. The other structural parameters are $a = 0.5$ mm, $b = 0.3$ mm, $w_1 = 0.3$ mm, and $w_2 = 0.2$ mm.

We first consider the case when the length $l_x = 1.49$ mm is fixed. Figures 2(c) and 2(d) show the transmission amplitude and phase spectra of the unit cells, with l_x varying from 0.82 to 1.88 mm for x- and y-polarized incidence. We see that for y-polarized excitation, the transmission magnitude of each unit cell has a transmission amplitude higher than 0.63 at 26 GHz, while the transmission phases show clear differences at the frequencies of interest. Particularly, the unit cells with $l_y = 0.82$, 1.49, 1.73, and 1.88 mm have four representative phases with a step of 90° at 26 GHz. On the contrary, for x-polarized excitation, both amplitude and phase curves do not show clear changes when varying the length l_y, indicating that the unit cell exhibits an extremely weak crosstalk between the two orthogonal linear polarization states. Similar results can be extracted when l_x varies and l_y remains fixed. This implies that the change of l_x will not affect the transmission performance of the meta-atom for the y-polarized illumination

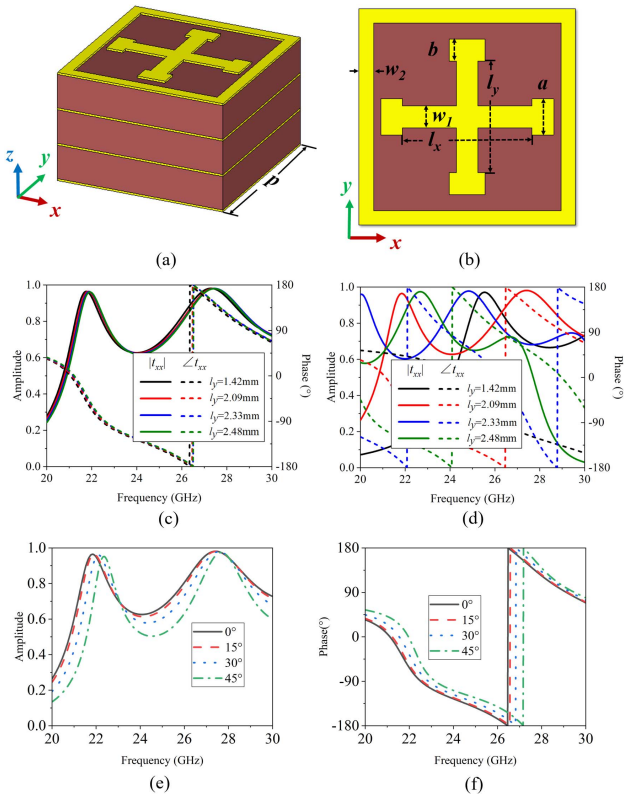

Fig. 2. (a) 3D view and (b) top view of the designed metasurface unit. Magnitude and phase spectra of the meta-atoms with different lengths l_y under (c) x-polarization excitation or (d) y-polarization excitation. The simulated (e) magnitude and (f) phase of the unit cell with $l_x = l_y = 2.09$ mm under x-polarization excitation in different incident angles.

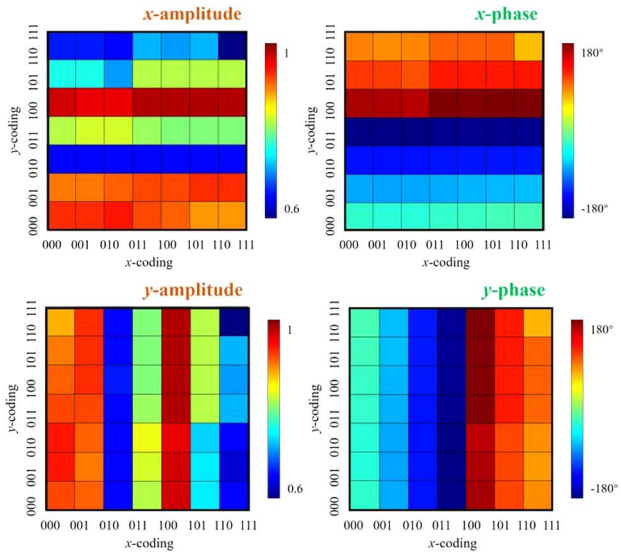

Fig. 3. Magnitudes and phases of the transmission coefficients obtained by 2D scanning simulation in x and y polarizations.

and vice versa, that is, the transmission amplitudes and phases of x- and y-polarized electromagnetic waves can be individually controlled by using such orthogonal I-shaped structures by varying l_x and l_y. As such, we can make use of such unit cells for designing metasurfaces with multi-polarization channels.

We further discuss the angular tolerance of the designed unit cells under oblique incidence. To simplify the problem, we only analyze one polarization and regard the other polarization as the equivalent since the two polarization states have same responses. The transmission amplitude and phase responses of the unit cell with $l_x = l_y = 2.09$ mm under x-polarization excitation are illustrated in Figs. 2(e) and 2(f). It is seen that both the transmission amplitude and phase curves are almost completely overlapped with each other for oblique incidence angles from 0° to 45°, which ensures very good angular stability of the proposed unit cell.

In order to achieve full phase coverage, unit cells with different transmission phase responses are designed and optimized. The unit has two independent and stable phase responses in the two orthogonal linear polarizations. The phase responses change with the element lengths l_x and l_y corresponding to x- and y-polarizations, respectively. Here, three-bit quantization is applied to avoid using the unit cell phase responses that change sharply with the unit cell structure. The precise core parameters l_x and l_y, corresponding to the three-bit quantization phases of the unit cell in the two polarizations, are obtained by parameter sweeping, and the lengths l_x and l_y as 0.60, 0.82, 1.20, 1.49, 1.63, 1.73, 1.78, and 1.88 mm are to mimic codings "000", "001", "010", "011", "100", "101", "110", and "111". The corresponding amplitudes and phases, obtained by simulations, of the two orthogonal linearly polarized transmission coefficients t_{xx} and t_{yy} at 26 GHz are presented in Fig. 3. It is clearly shown that all unit cells maintain a normalized amplitude above 0.63 and cover the 360° phase range with an interval of 45° under both the x- and y-polarized excitations. The same transmission coefficients have been observed from the results in two polarizations. The reasons may be the symmetry of the structure and the characters of the cross-dipole element. We can conclude that the phase responses in the two orthogonal directions are related to the lengths of l_x and l_y independently, which makes the polarization multiplexing possible. Unit cells with LP to co-LP, LP to RCP, LP to LCP, and LP to cross-LP conversions exhibit constant phase differences of 0°, 90°, −90°, and 180° between the two orthogonal polarization states t_{xx} and t_{yy}, respectively. Therefore, if a 45° polarized wave illuminates on these unit cells, the outgoing wave could not only realize arbitrary wavefront control, but also convert its polarization as well.

3. PHYSICAL IMPLEMENTATION OF THE METASURFACE HOLOGRAM DESIGN

To validate the performance of the proposed unit cell, a proof-of-concept demonstration of a four-channel transmission-type meta-hologram was designed and implemented. This metadevice can redirect the transmitted wave into the six preset focal spots with four representative polarization states. In our design, a polarization multiplexing supercell consisting of 2 × 2 meta-atoms is adopted to construct a multi-channel metasurface providing different spatial multiplexing. CST Microwave Studio is

utilized to model and simulate the proposed digital coding metasurface. The top view of a part of designed metasurface is shown in Fig. 4(a), and the inset is the top view of a supercell. To make the alignment easier in measurement, we rotate the orthogonal I-shaped resonators by 45° counterclockwise except the isotropic ones. After such rotation, the supercells can convert the polarization state of the x-polarized incident wave into x, y, right-handed circular, and left-handed circular polarizations in different channels.

The designed metasurface consists of 25×25 supercells along the x and y directions with a physical dimension of 150 mm × 150 mm, which is large enough to reconstruct a good microwave hologram image. The target hologram image is depicted in Fig. 4(b), where six focusing points A (A_1 and A_2), B, C (C_1 and C_2), D at the plane $z = 80$ mm, refer to x, y, left-handed circular, and right-handed circular polarizations, respectively. In our design, the electric field intensities at the points B and D are intentionally set as twice of those at the four points A_1, A_2, C_1, and C_2. To achieve the desired electromagnetic field shaping, the phase distribution across the metasurface is calculated by a holographic algorithm [29]. The spatial field distribution emitted from the metasurface can be written as

$$U(x_m, y_m, z_m) = \sum_{n=1}^{N} \frac{A(x_m, y_m, 0)}{r_n^m} \exp\{j[\varphi(x_m, y_m, 0) - kr_n^m]\}, \tag{3}$$

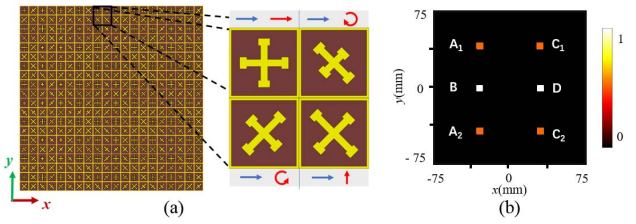

Fig. 4. (a) Top view of a part of metasurface and whole supercell. (b) Target focus image.

where r_n^m is the distance between the n-th unit cell at $(x_n, y_n, 0)$ and the m-th focal point at (x_m, y_m, z_m), k is the free-space wave number, and $A(x_m, y_m, 0)$ and $\varphi(x_m, y_m, 0)$ are the transmission amplitude and phase of the n-th unit cell, respectively. The angle of $U(x_m, y_m, z_m)$ gives the phase distributions required for reproducing the pre-designed patterns.

In this way, the problem of achieving the desired specific multi-focus pattern is transformed to calculate the unit cell sequences of the metasurface. Next, we employ an iterative approach to obtain the advisable phase patterns of meta-atoms via the corresponding diffraction operations of Eq. (3). Figures 5(a)–5(d) depict the target focus images for x-LP, y-LP, LCP, and RCP, and Figs. 5(e)–5(h) show corresponding four spatial phase profiles of 25×25 pixel arrays calculated by MATLAB, which can be derived from the spatial changes of l_x and l_y of each unit cell.

Theoretically, in the total electric field amplitude distribution, the electric field amplitude intensity of the two preset focusing points B and D is twice that of point A_1, point A_2, point C_1, and point C_2. In the electric field component amplitude distribution, for each polarization component, the focusing points corresponding to the orthogonal polarization vanish, and the electric field amplitude of the other cross-polarized focusing points should be $\sqrt{2}/2$ that of the original polarized focusing point.

In the simulation process, the metasurface is numerically modeled with open boundary conditions along x- and y-axes, and illuminated by a normally incident x-polarized plane wave at 26 GHz. We analyze the polarization states of the electromagnetic wave converging to each holographic point, obtain electric field components with polarization along the x- and y-axes directly through simulation, and get LCP and RCP components through further calculation as $E_l = \frac{1}{\sqrt{2}}(E_x - iE_y)$ and $E_r = \frac{1}{\sqrt{2}}(E_x + iE_y)$. Figure 6 shows the simulated normalized electric patterns. The pattern of E_x reconstructs all points except point B with y polarization [Fig. 6(a)]. The pattern of E_y reconstructs all points except points A_1 and A_2 with x polarization [Fig. 6(b)]. The pattern of E_l reconstructs all points

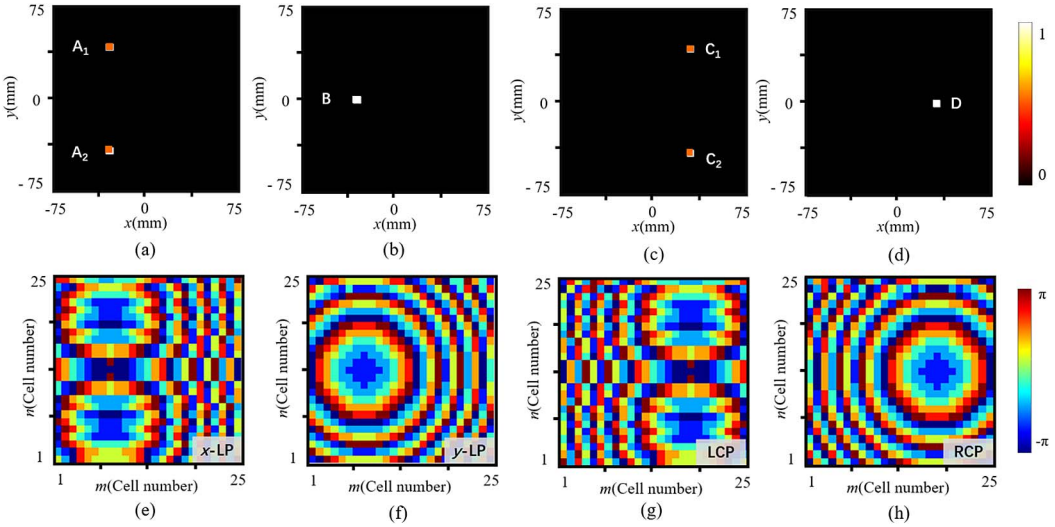

Fig. 5. (a)–(d) Target focus images and (e)–(h) corresponding required phase distributions for x-LP, y-LP, LCP, and RCP points.

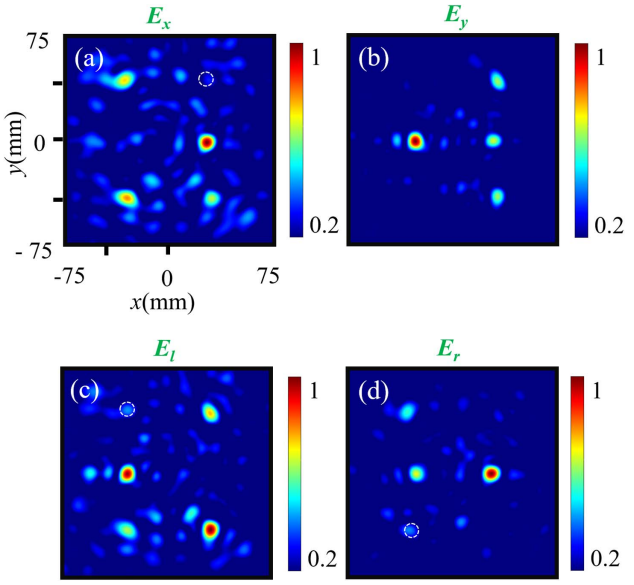

Fig. 6. Simulated normalized magnitude distribution of (a) E_x, (b) E_y, (c) E_l, and (d) E_r components at 26 GHz.

except point D with RCP [Fig. 6(c)]. The pattern of E_r reconstructs all points except points C_1 and C_2 with LCP [Fig. 6(d)]. For each electric field component, the holographic points with orthogonal polarization state disappear, which further proves that the crosstalk is very weak. This also indicates that the transmitted fields corresponding to points A, B, C, and D have x-linear, y-linear, left-handed circular, and right-handed circular polarizations, respectively. There are a few discrepancies between the simulated intensities of some cross-polarized focusing points in Fig. 6 and the theoretical values that may be caused by the non-uniform transmission amplitude and phase discontinuity of meta-atoms at the frequency of interest. Nevertheless, the simulation results are generally consistent with the theoretical design.

4. EXPERIMENTAL VALIDATION

To verify the actual effect of the metasurface hologram, a metasurface sample is fabricated using the standard printed circuit board (PCB) technique, as shown in Fig. 7(a). The experiment setup, as depicted in Fig. 7(b), is employed to detect the electric field distributions of the transmitted wave. The prototype is measured in a near-field microwave anechoic chamber, and absorbing material is placed around the open-ended rectangular waveguide probe to absorb the unnecessary electromagnetic waves. An antenna as a source and a probe as a receiver are linked to a vector network analyzer (Agilent Technologies, E8363B). An emitting horn antenna generates a linearly polarized quasi-plane beam at 26 GHz, which directly illuminates onto the metasurface. The observation plane is with a distance of 80 mm away from the metasurface. A waveguide probe is used to detect the area of 200 mm × 200 mm with a step of 2 mm.

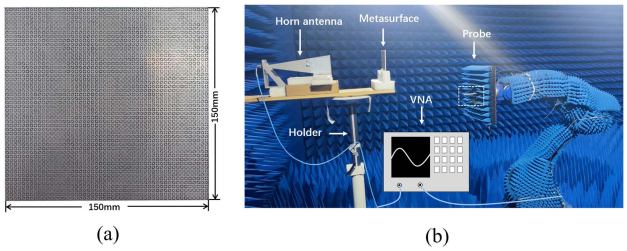

Fig. 7. (a) Fabricated metasurface sample and (b) experimental setup.

Figure 8 shows the measured intensities of the electric fields of E_x, E_y, E_l, and E_r at 26 GHz. It can be clearly observed that the metasurface realizes the polarization multiplexing hologram, and the results match well with the simulation ones. The comparison of normalized simulated and measured intensity curves of E_x, E_y, E_l, and E_r at 26 GHz is depicted in Fig. 9, and the high degree of coincidence of the curve trend further proves that the simulation and measured results are in good agreement. It is undeniable that the digital metasurface can well exhibit the effects of the polarization-multiplexing hologram.

Next, the theoretical, simulated, and measured normalized field distributions of the transmitted waves are shown in Fig. 10. Figure 10(a) depicts a theoretical preset normalized electric field distribution pattern, where most of the output energy is evenly concentrated in the six preset focusing points. Figures 10(b) and 10(c) demonstrate the synthetic simulated pattern and measured pattern, respectively, both of which are calculated by $E = \sqrt{E_x^2 + E_y^2}$. They show six simulated and measured holographic points, at the plane $z = 80$ mm, which are in good agreement with the theoretical designs. It can also be seen that some focal points in the figure are weaker than others, which means that the pattern has some local unevenness. These results show that the metasurface binds the energy of the electromagnetic wave to the target area well and generates patterns with high imaging quality.

Furthermore, the efficiency of the meta-device is evaluated. The imaging efficiency, i.e., diffraction efficiency, represents

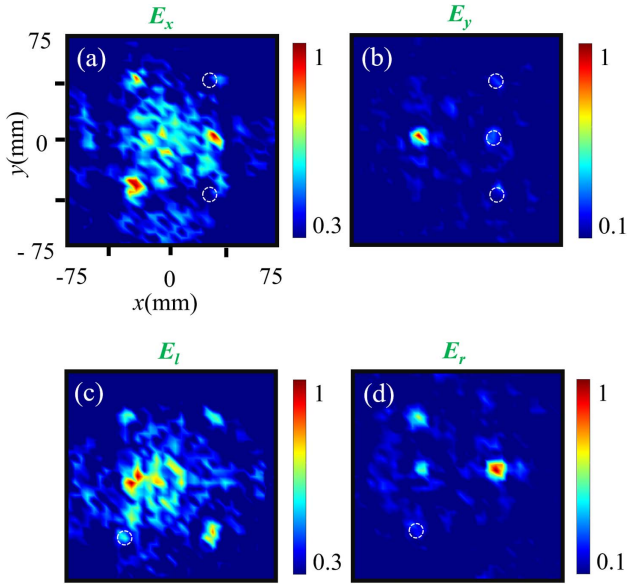

Fig. 8. Measured normalized magnitude distribution of (a) E_x, (b) E_y, (c) E_l, and (d) E_r components at 26 GHz.

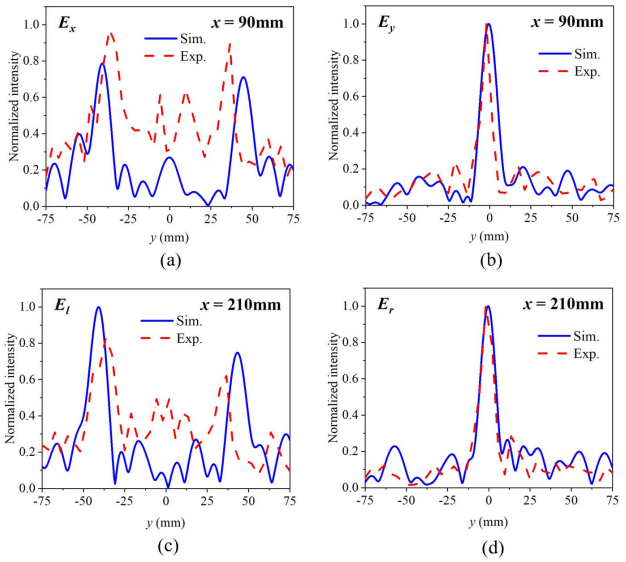

Fig. 9. Simulated and measured normalized amplitude curves of (a) E_x, (b) E_y, (c) E_l, and (d) E_r at 26 GHz.

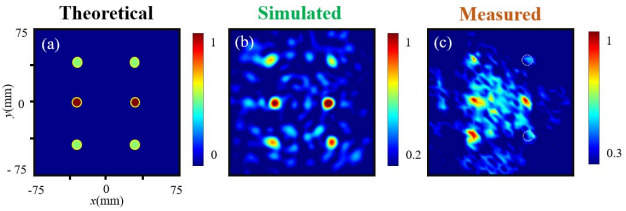

Fig. 10. Normalized magnitudes distributions of (a) theoretical, (b) simulated, and (c) measured combined electric transmitted field at 26 GHz.

how much energy is converted to the desired focal point, which is defined by the ratio of energy in the main focal spot region to the total transmitted energy. They are evaluated for the metasurface over a plane 150 mm × 150 mm at $z = 80$ mm. In the calculation process, the radius of each focal point is set to be $\lambda/2$, which can almost include most of the energy gathered at the point. The efficiency of the meta-device is found to be 51% for the simulation and 40% for the measurement.

The deviation between the simulated and measured results could be attributable to the manufacturing errors and limited size of the metasurface sample. Other possible reasons could be the wave generated by source antenna not being a pure plane wave. Maybe with the help of dielectric lens, the experimental results can be improved. In short, the multi-focus holographic image has been well reconstructed by transmitted waves in each polarization channel in both simulations and measurements.

5. CONCLUSION

In summary, we propose a general method for achieving independent wavefront manipulation with different polarization conversions in a single transmission-type metasurface. We propose an anisotropic orthogonal I-shaped resonator, which can manipulate the propagation phase and polarization of transmitted waves independently by changing the core size parameters of resonators. As a proof of concept, we design and fabricate a transmission-type metasurface for displaying polarization multiplexing multi-focus holograms, which can convert the incident linearly-polarized wave into arbitrary polarization at the same time and realize different wavefront manipulations. The design was further characterized numerically and experimentally, and the measured results have a good match with the simulation results. This work is important progress in the realization of transmission-type metasurfaces with efficient independent electromagnetic wave manipulation in multi-polarization channels. Compared with reflection-type metasurfaces, our metasurface can be applied to scenes with special requirements, and is expected to achieve new features that cannot be achieved by traditional design methods.

Funding. National Natural Science Foundation of China (62071291).

Disclosures. The authors declare no conflicts of interest.

Data Availability. Data underlying the results presented in this paper are not publicly available at this time but may be obtained from the authors upon reasonable request.

†These authors contributed equally to this work.

REFERENCES

1. N. I. Zheludev, "The road ahead for metamaterials," Science **328**, 582–583 (2010).
2. V. G. Veselago, "The electrodynamics of substance with simultaneously negative values of ϵ and μ," Physics-Uspekhi **10**, 509 (1968).
3. J. Pendry, A. Holden, D. Robbins, and W. Stewart, "Magnetism from conductors and enhanced nonlinear phenomena," IEEE Trans. Microw. Theory Tech. **47**, 2075–2084 (1999).
4. N. K. Grady, J. E. Heyes, D. R. Chowdhury, Y. Zeng, M. T. Reiten, A. K. Azad, A. J. Taylor, D. A. R. Dalvit, and H.-T. Chen, "Terahertz metamaterials for linear polarization conversion and anomalous refraction," Science **340**, 1304–1307 (2013).
5. J. B. Pendry, A. J. Holden, W. J. Stewart, and I. I. Youngs, "Extremely low frequency plasmons in metallic mesostructures," Phys. Rev. Lett. **76**, 4773–4776 (1996).
6. F. Zhou, Y. Bao, W. Cao, C. T. Stuart, J. Gu, W. Zhang, and C. Sun, "Hiding a realistic object using a broadband terahertz invisibility cloak," Sci. Rep. **1**, 78 (2011).
7. H. Tao, N. I. Landy, C. M. Bingham, X. Zhang, R. D. Averitt, and W. J. Padilla, "A metamaterial absorber for the terahertz regime: design, fabrication and characterization," Opt. Express **16**, 7181–7188 (2008).
8. M. R. Akram, G. Ding, K. Chen, Y. Feng, and W. Zhu, "Ultrathin single layer metasurfaces with ultra-wideband operation for both transmission and reflection," Adv. Mater. **32**, 1907308 (2020).
9. J. Ding, S. An, B. W. Zheng, and H. L. Zhang, "Multiwavelength metasurfaces based on single-layer dual-wavelength meta-atoms: toward complete phase and amplitude modulations at two wavelengths," Adv. Opt. Mater. **5**, 1700079 (2017).
10. X. Bai, F. Zhang, L. Sun, A. Cao, X. Wang, F. Kong, J. Zhang, C. He, R. Jin, W. Zhu, and T. J. Cui, "Radiation-type programmable metasurface for direct manipulation of electromagnetic emission," Laser Photon. Rev. **16**, 2200140 (2022).
11. X. Bai, F. Zhang, L. Sun, A. Cao, J. Zhang, C. He, L. Liu, J. Yao, and W. Zhu, "Time-modulated transmissive programmable metasurface for low sidelobe beam scanning," Research **2022**, 9825903 (2022).

12. L. Liu, X. Zhang, M. Kenney, X. Su, N. Xu, C. Ouyang, Y. Shi, J. Han, W. Zhang, and S. Zhang, "Broadband metasurfaces with simultaneous control of phase and amplitude," Adv. Mater. **26**, 5031–5036 (2014).
13. J. Y. Dai, J. Zhao, Q. Cheng, and T. J. Cui, "Independent control of harmonic amplitudes and phases via a time-domain digital coding metasurface," Light Sci. Appl. **7**, 90 (2018).
14. K. Katare, S. Chandravanshi, A. Sharma, A. Biswas, and M. J. Akhtar, "Anisotropic metasurface-based beam-scanning dual-polarized fan-beam integrated antenna system," IEEE Trans. Antennas Propag. **67**, 7204–7215 (2019).
15. M. I. Khan, Z. Khalid, and F. A. Tahir, "Linear and circular-polarization conversion in X-band using anisotropic metasurface," Sci. Rep. **9**, 4552 (2019).
16. L. Shao, D. Zhang, J. Liu, J. Zhang, Z. Li, X. Wang, and W. Zhu, "Single-layer noninterleaved metasurface for arbitrary vector beam conversion in triple bands," ACS Appl. Electron. Mater. **4**, 443–451 (2022).
17. R. Xie, G. Zhai, X. Wang, D. Zhang, L. Si, H. Zhang, and J. Ding, "High-efficiency ultrathin dual-wavelength Pancharatnam-Berry metasurfaces with complete independent phase control," Adv. Opt. Mater. **7**, 1900594 (2019).
18. L. W. Wu, H. F. Ma, R. Y. Wu, Q. Xiao, Y. Gou, M. Wang, Z. X. Wang, L. Bao, H. L. Wang, Y. M. Qing, and T. J. Cui, "Transmission-reflection controls and polarization controls of electromagnetic holograms by a reconfigurable anisotropic digital coding metasurface," Adv. Opt. Mater. **8**, 2001065 (2020).
19. Z. Li, D. Zhang, J. Liu, J. Zhang, L. Shao, X. Wang, R. Jin, and W. Zhu, "3-D manipulation of dual-helical electromagnetic wavefronts with a noninterleaved metasurface," IEEE Trans. Antennas Propag. **70**, 378–388 (2022).
20. Z. Li, X. Kong, J. Zhang, L. Shao, D. Zhang, J. Liu, X. Wang, W. Zhu, and C.-W. Qiu, "Cryptography metasurface for one-time-pad encryption and massive data storage," Laser Photon. Rev. **16**, 2200113 (2022).
21. J. Hao, Y. Yuan, L. Ran, T. Jiang, J. A. Kong, C. T. Chan, and L. Zhou, "Manipulating electromagnetic wave polarizations by anisotropic metamaterials," Phys. Rev. Lett. **99**, 063908 (2007).
22. H. L. Zhu, S. W. Cheung, K. L. Chung, and T. I. Yuk, "Linear-to-circular polarization conversion using metasurface," IEEE Trans. Antennas Propag. **61**, 4615–4623 (2013).
23. H. F. Ma, G. Z. Wang, G. S. Kong, and T. J. Cui, "Broadband circular and linear polarization conversions realized by thin birefringent reflective metasurfaces," Opt. Mater. Express **4**, 1717–1724 (2014).
24. B. Q. Lin, J. X. Guo, B. G. Huang, L. B. Fang, P. Chu, and X. W. Liu, "Wideband linear-to-circular polarization conversion realized by a transmissive anisotropic metasurface," Chin. Phys. B **27**, 054204 (2018).
25. L. Shao, M. Premaratne, and W. Zhu, "Dual-functional coding metasurfaces made of anisotropic all-dielectric resonators," IEEE Access **7**, 45716–45722 (2019).
26. T. Yan, Q. Ma, S. Sun, Q. Xiao, I. Shahid, X. Gao, and T. J. Cui, "Polarization multiplexing hologram realized by anisotropic digital metasurface," Adv. Theory Simul. **4**, 2100046 (2021).
27. L. Shao, Z. Li, Z. Zhang, X. Wang, and W. Zhu, "Multi-channel metasurface for versatile wavefront and polarization manipulation," Adv. Mater. Technol. **7**, 2200524 (2022).
28. J. Yang, X. Wu, J. Song, C. Huang, Y. Huang, and X. Luo, "Cascaded metasurface for simultaneous control of transmission and reflection," Opt. Express **27**, 9061–9070 (2019).
29. Z. Li, J. Qi, W. Hu, J. Liu, J. Zhang, L. Shao, C. Zhang, X. Wang, R. Jin, and W. Zhu, "Dispersion-assisted dual-phase hybrid meta-mirror for dual-band independent amplitude and phase controls," IEEE Trans. Antennas Propag. **70**, 7316–7321 (2022).